

## MICROWAVE LOSSES IN KINETIC-INDUCTANCE DEVICES FABRICATED FROM NbCN/MgO/NbCN TRILAYERS

K. R. Carroll, J. M. Pond, and E. J. Cukauskas  
Naval Research Laboratory  
Washington DC 20375

*Abstract*-- The microwave losses in kinetic-inductance devices fabricated from niobium carbon nitride/magnesium oxide/niobium carbon nitride (NbCN/MgO/NbCN) trilayers are being investigated. For microwave applications, these devices are attractive because of the substantial reduction in size over conventional superconductor architectures while maintaining low dispersion, wide bandwidth, and acceptable superconductor losses. Except for temperatures very near the critical temperature, the performance of these devices is presently limited to quality factors between 100-500 by losses in the dielectric. While this level of loss is acceptable for some applications, reduction in the dielectric loss is needed. For this study, MgO was chosen since this material can grow epitaxially on NbCN and is consequently expected to have loss tangents closer to those of bulk crystals. In addition to the dielectric losses, the superconductor losses and other film and device parameters will be reported.

### I. INTRODUCTION

For microwave applications of superconductivity, the use of kinetic-inductance devices is potentially attractive because of the substantial size reduction that is achievable in a microstrip or stripline device configuration. A factor of 30 reduction in the phase velocity has been previously demonstrated which roughly corresponds to a similar length reduction over conventional microstrip superconducting devices [1]. While kinetic-inductance devices have demonstrated low superconducting loss,  $\sim 50\text{-}\Omega$  characteristic impedance, low dispersion and wide bandwidth, the primary limitation has been the losses of the dielectric for both low- and high-temperature superconductors [1-4].

In this work, the dielectric and superconductor losses of niobium carbon nitride/magnesium oxide/niobium carbon nitride (NbCN/MgO/NbCN) trilayers are measured. The choice of dielectric was motivated by the low loss tangents of bulk crystalline material and the good lattice match to the NbCN superconducting films [5]. Since the growth of the NbCN is polycrystalline [6], with the proper deposition parameters, low-loss polycrystalline MgO should be achievable. For crystalline bulk MgO, loss tangents as low as  $10^{-5}$  have been observed for temperatures below 250 K [7].

A seven-pole high-frequency stub filter was used to determine the properties of the trilayer films. Fig. 1 shows a photograph of the filter where the resonant elements consist of the stub microstrip sections and the microstrip sections between the stubs. The basic principle of operation is that reflections of the signals at the end of the stubs interfere with those in the trunk line. When the signals are in phase, a

maximum in the transmission characteristics occurs and when they are out of phase, there is a null. Electrical transition between the  $50\text{-}\Omega$  coax measurement cables and the superconducting microstrip is facilitated by the tapered coplanar section of the superconductors at the input and output of the device.

For microstrip lines in the kinetic-inductance limit, a parallel plate description is applicable since the film thicknesses can easily be made one or two orders of magnitude less than the line widths. This analysis results in a phase velocity given by [8]

$$v_p = \frac{c}{\sqrt{\epsilon_r}} \frac{1}{\sqrt{1 + 2(\lambda/d_d)\coth(d_s/\lambda)}} \quad (1)$$

where  $c$  is the speed of light in vacuum,  $\lambda$  is the penetration depth,  $\epsilon_r$  the relative dielectric constant,  $d_d$  is the thickness of the dielectric, and  $d_s$  is the thickness of the superconductor. For extreme geometries where the film thicknesses are significantly smaller than a penetration depth, there is a large slowing of the wave over the value of the dielectric phase velocity. For our measurements, a Gorter-Casimir temperature dependence will be sufficient for the penetration depth:

$$\lambda = \frac{\lambda_0}{\sqrt{1 - (T/T_c)^4}} \quad (2)$$

where  $T$  is the temperature and  $T_c$  is the critical temperature of the superconductors.

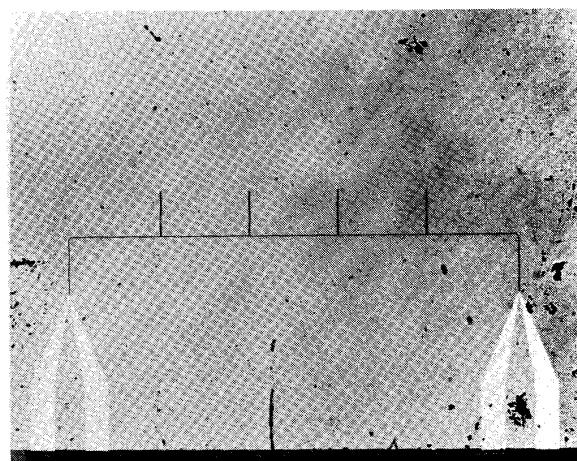


Fig. 1. Photograph of the high-frequency stub filter.

A convenient figure of merit for quantifying the losses in transmission lines is the quality factor  $Q$ . This quantity relates the amount of energy stored to that lost per oscillation of a propagating wave and is given by

$$Q = \pi f / v_p \alpha \quad (3)$$

where  $\alpha$  is the sum of attenuation coefficients of the superconductors  $\alpha_s$  and the dielectric  $\alpha_d$ . The effective attenuation coefficients for superconducting parallel plate transmission line can be related to the film parameters as follows [8]:

$$\alpha_s = \frac{(2\pi f)^2 \lambda^3 \mu_0 \epsilon_r \sigma v_p}{2d_d c^2} \left[ \coth(d_s/\lambda) + \frac{d_s}{\lambda} \sinh^{-2}(d_s/\lambda) \right] \quad (4)$$

$$\alpha_d = \frac{\pi f}{v_p} \tan \delta \quad (5)$$

where  $\mu_0$  is the permeability of free space,  $\tan \delta$  is the loss tangent, and the conductivity is given by

$$\sigma = \sigma_n \left( \frac{T}{T_c} \right)^4 \quad (6)$$

with  $\sigma_n$  the normal-state conductivity.

In the thin-film limit where  $d_d, d_s \ll \lambda$ , Eq. 3 becomes

$$Q_s = \frac{1}{4\pi f \mu_0 \sigma \lambda^2} \quad (7)$$

which is independent of film thicknesses. Consequently by reducing the film thicknesses, additional reduction in the phase velocity can be achieved without incurring any additional loss penalty. In Fig. 2, the quality factor is plotted in this limit for  $\sigma_n = 10^6 (\Omega m)^{-1}$  and  $\lambda_0 = 300$  nm. With these parameters and a dielectric loss tangent of  $10^{-5}$ , the superconductor would provide the dominant loss mechanism above 1.0 GHz even at  $0.3 T_c$ . For kinetic-inductance devices using a silicon dielectric, the quality factors have been between 100-500 depending on the frequency [1, 2, 4]. In the high-frequency range of the stub filter near 10 GHz, the  $Q$  is  $\sim 125$ . As will be seen in the following sections, this value has been improved with a MgO dielectric by about a factor of 3.

## II. FILM DEPOSITION AND CHARACTERIZATION

The deposition procedure and processing of the trilayer films is almost identical to that reported previously [2,4]. In an ultra-high vacuum system, 25 nm of NbCN and 50 nm of MgO were rf sputtered onto a quartz substrate. For the NbCN, a niobium target was used with a rf power density of 4.3 W/cm<sup>2</sup>, a 1.0 Pa gas mixture of argon (84%), nitrogen (13%), and methane (3%). When the MgO target was sputtered with Ar gas, the power density was 1.7 W/cm<sup>2</sup> which yielded a deposition rate of 3.5 nm/min.. The substrate temperature for

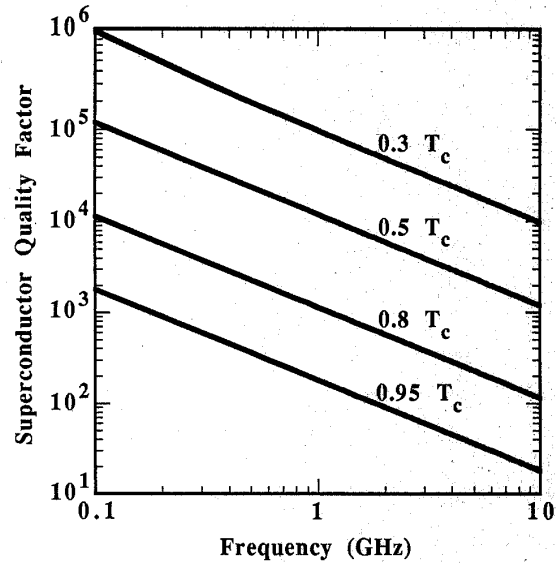


Fig. 2. Superconductor quality factor versus the frequency for a  $\sigma_n = 10^6 (\Omega m)^{-1}$  and  $\lambda_0 = 300$  nm in the thin-film limit.

both films was 600 C. After removing the substrate from the chamber, the coplanar transition region of the ground plane was defined using standard photolithographic steps and etched with an acid solution of HF, HNO<sub>3</sub>, and HCl. After removing the photoresist, the remaining half of the MgO and 25 nm of NbCN were deposited with a substrate temperature of 600 C. This top layer of the transmission line was then processed where the etching was done in a reactive ion etcher.

To help characterize the MgO film, x-ray diffraction measurements were performed on bilayers consisting of 300-nm thick MgO films on top of various thicknesses of NbCN. While the expected NbCN peaks were observed, no diffraction peaks were observed for the magnesium oxide indicating that it was fine grained or amorphous. Most of the bilayers were deposited onto quartz substrates, although an attempt was made on an MgO substrate. For this measurement, the bilayer consisted of 300 nm of NbCN and 200 nm of MgO. A very small MgO peak was observed and was attributed to the substrate.

Although the rf sputtered MgO films were probably noncrystalline, better results were obtained by electron-beam evaporation. For these bilayers, NbCN was deposited as indicated above followed by the MgO which was deposited on a heated stage at 500 C in the cryopumped evaporator. The thickness of the NbCN was 200 nm and 300 nm for the MgO. As can be seen from the x-ray diffraction data in Fig. 3, small (111) and (200) MgO peaks are clearly visible. Hopefully, optimization of the deposition temperature will yield better film crystallinity that will result in a lower loss tangent than that achieved with the amorphous films discussed in the next section.

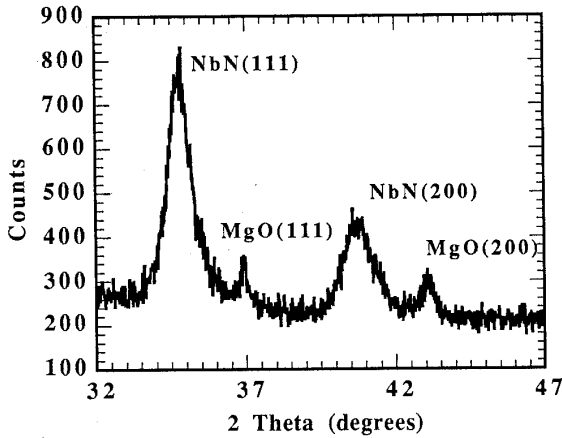


Fig. 3. X-ray counts versus the diffraction angle for a bilayer with films of sputtered NbCN and electron-beam evaporated MgO.

### III. MEASUREMENTS

The substrate containing the high frequency stub filter was mounted on an insert which provided coaxial cables that electrically connected the cryogenic environment to a Hewlett Packard 8510 network analyzer. Partial exposure of the center conductor at the cryogenic end allows pressure contact of the coax to the filter's coplanar transition region. Additional pressure contacts are also provided for the ground plane connections. The insert is enclosed in a double-walled vacuum which is immersed in liquid helium. A temperature controller stabilizes the device operating temperature by regulating the power delivered to a resistive heater on the substrate holder.

Figures 4 and 5 show the amplitude of the transmission characteristics  $S_{21}$  for the stub filter at the temperatures 4.66 K and 11.56 K respectively. The solid lines represent the measured data while the dashed lines are the results of the model discussed below. The maximum transmission of the response occurs at the pass band center frequencies  $f_c$  when the difference between the length of the stub  $l_s$  and the distance between the stubs  $l_t$  is half a wavelength. Consequently, the phase velocity  $v_p$  is given by

$$v_p = \frac{2f_c(l_t - l_s)}{m} \quad (8)$$

where  $m$  is an integer. With this equation, the transmission characteristics, and the dimensions  $l_t = 1.0$  mm and  $l_s = 0.5$  mm, the normalized phase velocity  $v_p/c$  as a function of temperature can be determined as shown in Fig. 6. The solid line represents the best fit to the phase velocity data using Eqs. 1 and 2. This analysis yielded  $\lambda_0 = 354$  nm and  $T_c = 13.2$  K which is consistent with values that have been determined previously. The other parameters required to perform this calculation where the relative dielectric constant of MgO  $\epsilon_r = 9.65$  [7], and the film thicknesses  $d_s = 25$  nm and  $d_d = 100$  nm.

While the passband location allows a determination of  $\lambda_0$  and  $T_c$ , a more sophisticated model of the device must be used to extract the loss information from the transmission characteristics. For the stub filter, one represents the stubs and the other sections of microstrip with general transmission lines elements with the appropriate lengths, the phase velocity given by Eq. 1, attenuation constants given by Eqs. 5 and 6, and an impedance given by

$$Z_c = \frac{d_d}{w} \left( \frac{c}{v_p \sqrt{\epsilon_r}} \right) \sqrt{\frac{\mu_0}{\epsilon_0 \epsilon_r}} \quad (9)$$

where  $\mu_0$  is permeability of free space and  $w$  is the line widths of 15.2  $\mu\text{m}$  and 7.2  $\mu\text{m}$  for the stub and trunk lines respectively. This characterization of the microstrip lines can be straight forwardly incorporated into Eesof's microwave circuit analysis program. A parasitic capacitance and inductance can be included in the model to account for the pressure contacts and the coplanar transition region. This model has been used previously with a number of kinetic-inductance devices with good results [2-4].

For the model responses shown in Figs. 4 and 5, a  $\tan\delta = 0.0031$  and  $\sigma_n = 1.7 \times 10^6 (\Omega\text{m})^{-1}$  were obtained where the uncertainty in the values is approximately 15 %. The response of the first pass band ( $f_c = 9.38$  GHz) at  $T = 4.66$  K determines the dielectric loss as would be expected from Fig. 2. Note that for this pass band, the model describes the ripple very well. This agreement was achieved by allowing the lengths of the resonant elements to vary by a maximum of 5%. Physically, this assumption is thought to be justified by a variation in the density of the dielectric. This variation implies an effective thickness variation along the sections of microstrip. While technically one should incorporate the thickness variation directly in the model, the error that results from neglecting the small fluctuation in line impedance is not expected to change the results significantly. This effect has been discussed in detail elsewhere [2].

This loss tangent for an amorphous MgO film represents approximately a factor of 3 improvement over that found for a stub filter with a hydrogenated silicon dielectric which also operated in a similar frequency range [4]. Hopefully, improvement in the MgO deposition process will decrease the dielectric losses. While lower loss tangents have been observed for Si:H films, these have been observed in devices which operate at lower frequencies [1, 2]. The values obtained for the conductivity are consistent with values previously found for NbCN.

Naturally, a long kinetic-inductance delay line is more suited for extracting the loss tangent of the dielectric. If the line is matched to the 50- $\Omega$  cables of the measurement system, the frequency dependence of the losses can be determined with modest effort. The primary advantage of the stub filter is that the lengths of the microstrip lines are relatively short. Consequently, defects in the substrate or pin holes that happen to lie on microstrip line are less likely to prevent microwave transmission by interrupting the continuity of the transmission lines.

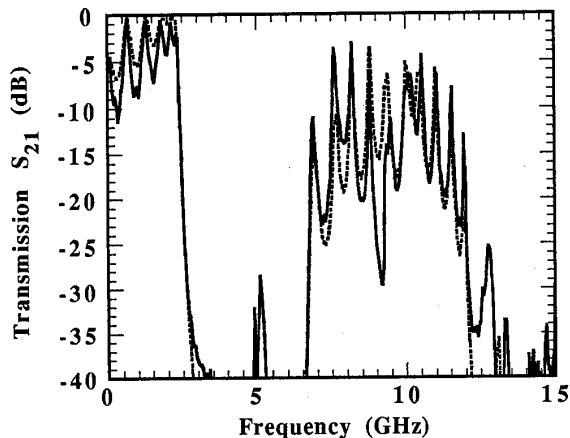


Fig. 4. Amplitude of the experimental (solid line) and modeled (dashed line) transmission characteristics at  $T = 4.66$  K

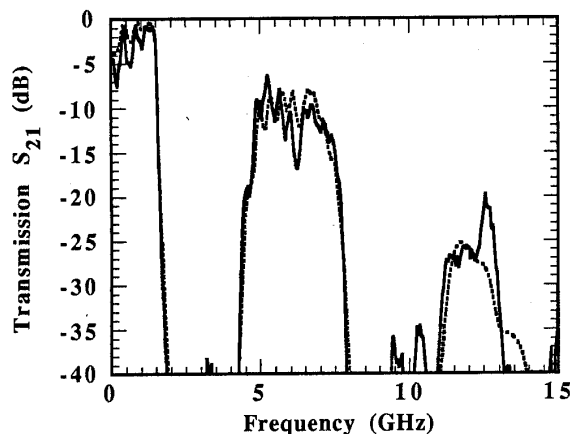


Fig. 5. Amplitude of the experimental (solid line) and modeled (dashed line) transmission characteristics at  $T = 11.67$  K.

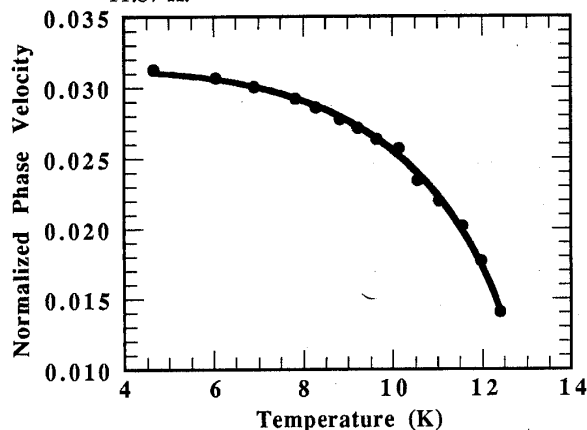


Fig. 6. Normalized phase velocity  $v_p/c$  of the stub filter versus the temperature. The dots represent the experimental data and the solid line is the best fit.

#### IV. CONCLUSIONS

The loss tangent of an amorphous MgO thin film has been measured for frequencies near 10 GHz with a kinetic-inductance stub filter. The value of 0.0031 represents a factor of  $\sim 3$  improvement over Si:H films found for a similar kinetic-inductance structure operating in a similar frequency range. Further improvement in the dielectric has also been discussed. Other properties of the superconducting trilayer structure were consistent with previous results.

#### ACKNOWLEDGEMENTS

The authors would like to thank Dr. John Talvacchio for useful discussions concerning the deposition of MgO. This work was supported in part by the Office of Naval Technology. One of the authors (KRC) held a National Research Council - Naval Research Laboratory Fellowship during the course of this work.

#### REFERENCES

- [1] J. M. Pond, J. H. Claassen, and W. L. Carter, "Kinetic inductance microstrip delay lines," *IEEE Trans. Magn.*, vol. 23, pp. 903-907, Mar. 1987; "Measurements and modeling of kinetic inductance microstrip delay lines," *IEEE Trans. on Microwave Theory Tech.*, vol. 35, 1256-1262, Dec. 1987.
- [2] K. R. Carroll, J. M. Pond and E. J. Cukauskas, "Superconducting kinetic inductance microwave filters" submitted to *IEEE Trans. Appl. Superconductivity*, Jan. 1992.
- [3] J. M. Pond, K. R. Carroll, J. S. Horwitz, D. B. Chrisey, M. S. Osofsky, and V. C. Cestone, "Penetration depth and microwave loss measurements with a  $\text{YBa}_2\text{Cu}_3\text{O}_{7-\delta}/\text{LaAlO}_3/\text{YBa}_2\text{Cu}_3\text{O}_{7-\delta}$  trilayer transmission line," *Appl. Phys. Lett.*, vol. 59, pp. 3033-3035, Dec. 1991.
- [4] J. M. Pond, K. R. Carroll, and E. J. Cukauskas, "Ultra-compact microwave filters using kinetic inductance microstrip," *IEEE Trans. Magn.*, vol. 27, 2696-2699, Mar. 1991.
- [5] J. Talvacchio and A. I. Braginski, "Tunnel junctions fabricated from coherent NbN/MgO/NbN and NbN/ $\text{Al}_2\text{O}_3$ /NbN structures," *IEEE Trans. Magn.*, vol. 23, pp. 859-862, Mar. 1987.
- [6] E. J. Cukauskas, W. L. Carter, and S. B. Qadri, "Superconducting and structure properties of niobium nitride prepared by rf magnetron sputtering," *J. Appl. Phys.*, vol. 57, pp. 2538-2542, Apr. 1985.
- [7] T. Konaka, M. Sato, H. Asano, and S. Kubo, "Relative permittivity and dielectric loss tangent of substrate materials for high- $T_c$  superconducting film," *J. Superconductivity*, vol. 4, pp. 283-288, 1991.
- [8] J. C. Swihart, "Field solution for a thin-film superconducting strip transmission line," *J. Appl. Phys.*, vol. 32, pp. 461-469, Mar. 1961.